Journal of Power Sources 224 (2013) 20–27

Contents lists available at SciVerse ScienceDirect

Journal of Power Sources

journal homepage: www.elsevier.com/locate/jpowsour

Advanced mathematical methods of SOC and SOH estimation for lithium-ion batteries

Dave Andre [a,*], Christian Appel [a], Thomas Soczka-Guth [a], Dirk Uwe Sauer [b]

[a] Deutsche ACCUmotive GmbH & Co. KG, 73230 Kirchheim u. Teck (Nabern), Germany
[b] Institute for Power Electronics and Electrical Drives (ISEA), RWTH Aachen University, 52066 Aachen, Germany

HIGHLIGHTS

- Advanced SOC and SOH estimation of a lithium-ion battery by a Dual Kalman filter in combination with support vector machine.
- Feasibility proof and validation by measured drive cycle data.
- Estimation accuracy far better than the reported ones (SOC error $< 0.5\%$).
- Real-time diagnosis by management system conceivable.

ARTICLE INFO

Article history:
Received 3 May 2012
Received in revised form
27 August 2012
Accepted 1 October 2012
Available online 6 October 2012

Keywords:
State of health
Lithium-ion battery
State of charge
Battery management system
Unscented Kalman filter
Support vector regression

ABSTRACT

Two novel methods to estimate the state of charge (SOC) and state of health (SOH) of a lithium-ion battery are presented. Based on a detailed deduction, a dual filter consisting of an interaction of a standard Kalman filter and an Unscented Kalman filter is proposed in order to predict internal battery states. In addition, a support vector machine (SVM) algorithm is implemented and coupled with the dual filter. Both methods are verified and validated by cell measurements in form of cycle profiles as well as storage and cycle ageing tests. A SOC estimation error below 1% and accurate resistance determination are presented.

1. Introduction

In automotive applications, the estimation of the actual state of charge (SOC) and state of health (SOH) of the battery is rather crucial to predict e.g. the availability of power and energy in hybrid electric vehicles (HEV) and electric vehicles (EV). During lifetime, the resistance as well as the capacity and in consequence SOC of every lithium-ion cell changes through electrochemical degradation processes like electrolyte decomposition or growth of a solid electrolyte interface (SEI) on the anode surface [1]. This variation is hard to measure directly in a vehicle, but has to be known for an accurate range and power prediction. Without a SOH correction or update by the battery management system (BMS), the driver will experiences an overestimated range or less acceleration.

Because of this necessity of a reliable SOC and SOH prediction, there were a lot of publications in the last few years. The application of Kalman filtering can be regarded as a state of the art technique. Usually Extended Kalman filtering is used (e.g. Ref. [2]), but also Unscented or Sigma-Point Kalman filtering is utilized (e.g. Ref. [3]).

The use of machine learning techniques, and especially support vector machines, has grown in popularity over the last few years, not only in SOC and SOH estimation [4–6] but in various application areas. A good overview of the state-of-art battery prognostic algorithms is given by Zhang and Lee [7], where not only Kalman filters and support vector machines, but also other techniques, such as neural networks or particle filters are presented.

This paper is based on the master thesis of Christian Appel and presents a novel method for SOC and SOH prediction using

* Corresponding author. Tel.: +49 (0)15158605924.
E-mail address: dave.andre@daimler.com (D. Andre).

0378-7753/$ – see front matter © 2012 Elsevier B.V. All rights reserved.
http://dx.doi.org/10.1016/j.jpowsour.2012.10.001

a standard Kalman filter for linear systems, an Unscented Kalman filter and machine learning techniques is presented. Due to its general structure and design; this approach, demonstrated at a nickel manganese cobalt (NMC) pouch cell, is valid independent of cell chemistry and design. Even if no direct understanding of the ageing mechanism or sources can be gained by such SOH algorithm, information can be collected about the caused degradation of particular ageing factors. Thus, the main factors can be identified and minimized by an optimized operation strategy on the BMS later on.

After the introduction and the presentation of the state of the art SOC and SOH estimation, a brief description of the mathematical methods used in this approach is given in the second section, followed by the description of the measurements and ageing test. The fourth section describes the implementation of the battery model and the application of the mathematical methods and subsequently the results are presented and discussed.

2. Mathematical methods

In this section a description of the mathematical methods applied in this study is given. Namely this is a standard Kalman filter, an Unscented Kalman filter and the support vector regression.

2.1. Kalman filter for linear systems

The first used technique will be the well-known Kalman filter (KF) for linear systems, developed by Kalman in 1960 [8]. A good introduction to Kalman filters can be found in Ref. [9]. Thus, only a presentation of the applied algorithm is given in this paper.

A n-dimensional linear dynamic discretized system of a discrete random process consists of the following:

(i) A process model:

$$\boldsymbol{x}_{k+1} = A_k\boldsymbol{x}_k + B_k u_k + \boldsymbol{v}_k, \tag{1}$$

where $\boldsymbol{x}_k$ is a discrete random process, which is called state vector, $A_k \in \mathbb{R}^{n\times n}$ the state transition matrix, $B_k \in \mathbb{R}^{n\times m}$ the control input matrix, $u_k \in \mathbb{R}^m$ a deterministic control vector and $\boldsymbol{v}_k$ an uncorrelated discrete random process, which is called process noise, where:

$$Q_k = E(\boldsymbol{v}_k\boldsymbol{v}_k^T)$$

(ii) An observation model:

$$z_k = H_k\boldsymbol{x}_k + \boldsymbol{w}_k, \tag{2}$$

where $H_k \in \mathbb{R}^{l\times n}$ is the observation matrix and $\boldsymbol{w}_k$ an uncorrelated discrete random process, which is called measurement noise, where:

$$R_k = E(\boldsymbol{w}_k\boldsymbol{w}_k^T)$$

Presuming that the following assumptions hold:

$$E(\boldsymbol{w}_k\boldsymbol{v}_j^T) = 0 \quad \forall j,k \tag{3}$$

$$E(\boldsymbol{w}_k\boldsymbol{x}_j^T) = 0 \quad \text{for } j \le k \tag{4}$$

$$E(\boldsymbol{v}_k\boldsymbol{x}_j^T) = 0 \quad \text{for } j \le k \tag{5}$$

Let $\widehat{\boldsymbol{x}}_k = \widehat{\boldsymbol{x}}(k|.k)$ the a posteriori state estimate and $P_k = P(k|k)$ be the a posteriori error covariance matrix at time step k, given measurements up to time step k, then the standard Kalman filter equations for the described linear system are the following:

(i) Calculate state estimate and estimate covariance prediction (a priori):

$$\widehat{\boldsymbol{x}}(k+1|k) = A_k\widehat{\boldsymbol{x}}(k|k) + B_k u_k$$
$$P(k+1|k) = A_k P(k|k)A_k^T + Q_k$$

(ii) Calculate innovation and innovation covariance:

$$r_{k+1} = \boldsymbol{z}_{k+1} - H_{k+1}\widehat{\boldsymbol{x}}(k+1|k)$$
$$S_{k+1} = H_{k+1}P(k+1|k)H_{k+1}^T + R_{k+1}$$

(iii) Calculate Kalman gain:

$$K_{k+1} = P(k+1|k)H_{k+1}^T S_{k+1}^{-1}$$

(iv) Calculate state estimate and estimate covariance update (a posteriori):

$$\widehat{\boldsymbol{x}}(k+1|k+1) = \widehat{\boldsymbol{x}}(k+1|k) + K_{k+1}r_{k+1}$$
$$P(k+1|k+1) = P(k+1|k) + K_{k+1}S_{k+1}K_{k+1}^T$$

2.2. Unscented Kalman filter

For our purpose a nonlinear extension to the Kalman filter is applied: the Unscented Kalman filter (UKF), using the unscented transformation as described in Ref. [10]. Rather than linearizing the nonlinear functions as in the Extended Kalman filter (EKF), the probability distribution will be approximated by a certain number of sigma points and those will be transformed by the nonlinear system functions to approximate the mean and covariance estimate.

The discretized general nonlinear dynamic system has the following form, analogous to the linear systems (1) and (2) and requiring assumptions (3)–(5) still hold:

(i) Process model:

$$\boldsymbol{x}_{k+1} = f_k(\boldsymbol{x}_k, u_k, \boldsymbol{v}_k) \tag{6}$$

(ii) Observation model:

$$z_k = h_k(\boldsymbol{x}_k, \boldsymbol{w}_k) \tag{7}$$

(i) Choose $n+1$ sigma points as follows:

$$\begin{aligned} x^{(0)} &= \bar{x} = E(x) \\ x^{(i)} &= x^{(0)} + \left(\sqrt{(n+\kappa)P}\right)_i^T, \quad i = 1,\ldots,n \\ x^{(n+i)} &= x^{(0)} - \left(\sqrt{(n+\kappa)P}\right)_i^T, \quad i = 1,\ldots,n, \end{aligned}$$

where $(\sqrt{(n+\kappa)P})_i$ is the ith row of the matrix square root $(\sqrt{(n+\kappa)P})$.

Weights of the sigma points are chosen as follows:

$$W^{(0)} = \frac{\kappa}{n+\kappa}$$

$$W^{(i)} = \frac{1}{2(n+\kappa)}, \quad i = 1,\ldots,2n$$

(ii) Calculate state estimate prediction (a priori):

$$\begin{aligned} x^{(i)}(k+1|k) &= f\left(x^{(i)}(k|k), u_k\right) + v_k \\ \hat{x}(k+1|k) &= \sum_{i=0}^{2n} W^{(i)} x^{(i)}(k+1|k) \end{aligned}$$

(iii) Calculate estimate covariance prediction (a priori):

$$\begin{aligned} P(k+1|k) = Q_k + \sum_{i=0}^{2n} W^{(i)} &\left[x^{(i)}(k+1|k) - \hat{x}(k+1|k)\right] \\ &\times \left[x^{(i)}(k+1|k) - \hat{x}(k+1|k)\right]^T \end{aligned}$$

(iv) Calculate innovation:

$$\begin{aligned} z^{(i)}(k+1|k) &= h\left(x^{(i)}(k+1|k), u_k\right) + w_k \\ \hat{z}(k+1|k) &= \sum_{i=0}^{2n} W^{(i)} z^{(i)}(k+1|k) \end{aligned}$$

(v) Calculate Kalman gain:

$$\begin{aligned} P_{yy}(k+1|k) &= R_k + \sum_{i=0}^{2n} W^{(i)} \left[z^{(i)}(k+1|k) - \hat{z}(k+1|k)\right] \\ &\left[z^{(i)}(k+1|k) - \hat{z}(k+1|k)\right]^T \\ P_{xy}(k+1|k) &= \sum_{i=0}^{2n} W^{(i)} \left[x^{(i)}(k+1|k) - \hat{x}(k+1|k)\right] \left[z^{(i)}(k+1|k) \right. \\ &\left. - \hat{z}(k+1|k)\right]^T \\ K_k &= P_{xy}(k+1|k) P_{yy}(k+1|k)^{-1} \end{aligned}$$

(vi) Calculate state estimate update (a posteriori):

$$\hat{x}(k+1|k+1) = \hat{x}(k+1|k) + K_k\left(z_k - \hat{z}(k+1|k)\right)$$

(vii) Calculate estimate covariance update (a posteriori):

$$P(k+1|k+1) = P(k+1|k) + K_k P_{yy}(k+1|k) K_k^T$$

2.3. Support vector regression

The second method used in this approach is the support vector regression (SVR). A comprehensive introduction can be found in Ref. [11]. Given a set of training data:

$$\{(x_1,y_1),(x_2,y_2),\ldots,(x_n,y_n)\} \subset \mathbb{R}^n \times \mathbb{R} \tag{8}$$

where $x_i \in \mathbb{R}^n$ are the input parameter vectors and $y_i \in \mathbb{R}$ are the target values, the task in the so-called ε-incentive support vector regression is to find a linear function

$$f(x) = \langle w, x\rangle + b \tag{9}$$

as flat as possible in the way that the values $f(x_i)$ have at most ε deviation from the targets y_i. Introducing "slack variables" ξ_i, ξ_i^* to create a "soft margin" and therefore allowing measurement errors and be able to cope with otherwise infeasible constraints, leads to a dual optimization problem. Utilizing the Karush–Kuhn–Tucker (KKT) condition, the parameter b in function $f(x)$ can be calculated. Obviously SOC and SOH prediction will not be a linear regression problem, so a method for the nonlinear case is required. Hereby, the idea is to transform the input data nonlinearly in a higher dimensional feature space F:

$$\begin{aligned} \phi &: \mathbb{R}^n \to F \\ x &\mapsto \phi(x) \end{aligned}$$

The equations in the dual optimization problem are solely dependent on inner products of the form $\langle x_i, x_j\rangle$. Hence in feature space it is sufficient to know

$$k(x_i,x_j) = \left\langle \phi(x_i), \phi(x_j)\right\rangle \tag{10}$$

with a so called kernel function k to represent an inner product in feature space and the nonlinear transformation ϕ has not be known explicitly. This is the kernel trick and Mercer's theorem (1909) gives a condition for such functions.

In this study an ε-incentive support vector regression is applied and Gaussian Kernels of the following form will be used:

$$k(x,y) := \exp\left(-\frac{\|x-y\|^2}{2\sigma^2}\right) \tag{11}$$

3. Experiments

In this section a description of the measurements taken for the present study and details of the used cell type are given.

High-energy lithium-ion pouch cells with a graphite anode and a NMC cathode were used. The cells have a nominal voltage of 3.6 V and a nominal capacity of 10 Ah.

In order to have the chance to validate the subsequent estimation, all cells were characterized by electrical parameter tests. Besides a capacity test with a C-rate of one, a pulse power characterization profile (PPCP), based on the "Hybrid Pulse Power Characterisation Test" of PNGV/FreedomCar and the EUCAR "Open Circuit Voltage and Power Determination Test" [12], is part of this characterization. It consists of a certain pulse power profile at different SOC steps, from 90%SOC down to 10% SOC in 10%SOC-steps. The pulse power profile procedure can be seen in Table 1.

The SOC–OCV curves, which are later required in the process model of filter 2, are obtained from the PPCP measurements as well as a time-dependent resistance

Table 1
Pulse power profile procedure.

Time increment	Cumulated time	Current rate
18 s	18 s	−4 C
40 s	58 s	0
10 s	68 s	3 C
40 s	108 s	0

$$R_{\Delta t} = \frac{U_{t_0} - U_{t_0+\Delta t}}{I_{t_0}} \tag{12}$$

which can be calculated for each SOC step.

The recorded measurement data can be divided into two different classes:

(i) Long-term cell ageing tests:A large amount of storage and cycle ageing tests were performed over more than one year with specific lithium ion cells. During the test duration, regular check-ups were conducted to record the capacity fade in the cells. The check-ups consist of standardized capacity and power tests as described above.
(ii) Short-term driving cycle cell measurements:The cells, which passed the ageing tests (i) and consequently have a different SOH, were used for two types of driving cycle measurements based on the FTP-72 cycle to simulate real world requirements:
(ii.a) Full-charged cells are completely discharged by FTP-72 load profiles.
(ii.b) Full-charged cells are discharged down to ca. 40% by a load profile consisting of FTP-72 cycles, pauses and a charge period.

The load profile based on the FTP-72 cycle and the load profile of the combined cycle measurements can be seen in Figs. 1 and 2, respectively. While, the first type of measurements is only used for having cells at different SOH with a known history and for the SVR application. The second type is used for a real-time SOC and SOH estimation.

4. Implementation

In this section the implemented battery model is introduced and the derivation of the Dual Kalman filter (DKF) and the application of the SVR algorithm is presented.

The underlying battery model is a state of the art electric equivalent circuit model with 2 RC members and is shown in Fig. 3 [13].

$$\begin{aligned} U_{\text{cell},k} &= U_{\text{OCV},k} + U_{\text{ohm},k} + U_{1,k} + U_{2,k} \\ &= U_{\text{OCV}}(\text{SOC}_k) + R_{\text{ohm},k} \cdot I_k + U_{1,k} + U_{2,k} \end{aligned} \tag{13}$$

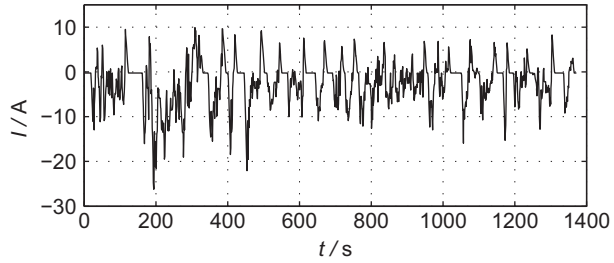

Fig. 1. Applied current load profile based on FTP-72 drive cycle.

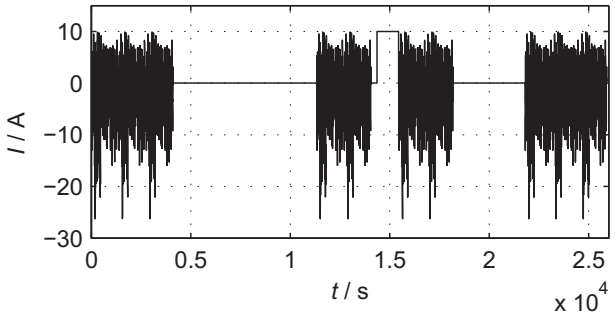

Fig. 2. Applied current load profile for combined cyclic measurements consisting of pauses, drive cycles and recharging with a total time of 7 h.

where $U_{\text{OCV},k}$ is the open-current voltage (OCV) at time step t_k. The OCV corresponds to a certain SOC, which is implemented by a non-linear characteristic curve $U_{\text{OCV}}(\text{SOC}_k)$. Moreover, this curve is assumed to be consistent over lifetime, if the SOC calculation is based on the actual, not the nominal, capacity. Furthermore the over-voltages U_1 and U_2 can be expressed by:

$$\begin{aligned} \underbrace{\begin{pmatrix} U_{1,k+1} \\ U_{2,k+1} \end{pmatrix}}_{x_{k+1}} &= \underbrace{\begin{pmatrix} e^{-\frac{\Delta t_{k+1}}{R_1 C_1}} & 0 \\ 0 & e^{-\frac{\Delta t_{k+1}}{R_2 C_2}} \end{pmatrix}}_{:=A_k} \underbrace{\begin{pmatrix} U_{1,k} \\ U_{2,k} \end{pmatrix}}_{=x_k} \\ &+ \underbrace{\begin{pmatrix} R_1\left(1 - e^{-\frac{\Delta t_{k+1}}{R_1 C_1}}\right) \\ R_2\left(1 - e^{-\frac{\Delta t_{k+1}}{R_2 C_2}}\right) \end{pmatrix}}_{:=B_k} \cdot \underbrace{I_k}_{=u_k} \end{aligned} \tag{14}$$

where $\Delta t_{k+1} := t_{k+1} - t_k$ is the time span between time step $k+1$ and k.

These equations will be implemented in both, the standard Kalman filter (filter 1) and the Unscented Kalman filter (filter 2).

The process model equation for the state of charge is:

$$\text{SOC}_{k+1} = \text{SOC}_k + \frac{I_k \cdot \Delta t_{k+1}}{C_{\text{cell}}} \cdot 100 \tag{15}$$

where I_k is the measured current at time step k, which is constant on the time interval $[t_k, t_{k+1}]$.

In this study, a combination of a standard Kalman filter and an Unscented Kalman filter is used. The first filter estimates the polarization over-voltage U_1, the diffusion over-voltage U_2 and the ohmic resistance R_{ohm}. The output of this filter is fed into the second filter, estimating SOC as well as the polarization and diffusion resistances R_1 and R_2. In the system model of the second filter, the actual cell capacity estimate of the SVR can be used to predict the SOC.

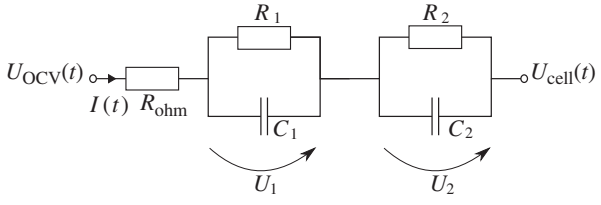

Fig. 3. Used electric equivalent circuit model of a lithium-ion cell and corresponding internal cell parameters.

Table 2
Equations for filter 1 (KF).

State vector	$\boldsymbol{x}_k = \begin{pmatrix} U_{1,k} \\ U_{2,k} \\ R_{\mathrm{ohm},k} \end{pmatrix}$
Control input	$u_k = I_k$
Observation	$z_k = U_{\mathrm{cell},k} - U_{\mathrm{OCV},k}$
Process model	$\boldsymbol{x}_{k+1} = A_k \cdot \boldsymbol{x}_k + B_k \cdot u_k$
Observation model	$z_k = (1\ 1\ I_k) \cdot \boldsymbol{x}_k$

The motivation for this Dual Kalman filter is based on three advantages:

- Decoupling of estimations, thus reduction of interactions and avoiding of building-ups of a filter
- Separation of variables, which cannot be estimated by a single filter
- Reduction of computation efforts, since two filters of lower dimensions are faster than one higher dimensional one [14]

Both filters use the input signal current and the measured cell voltage. Measurement data were obtained by the previously described driving cycle tests to simulate real world requirements. Therefore the dual filter can be used online, that means e.g. it can be implemented in the battery management system to predict the power and energy availability.

The equations for both filters can be found in Tables 2 and 3, respectively. The time constants $\tau_1 = R_1C_1$ and $\tau_2 = R_2C_2$ were assumed to be constant in both filters. This assumptions was rather made than keeping the capacities C_1 and C_2 constant, because of the fitting results and robustness considerations. The dual filter layout can be found in Fig. 4.

The actual cell capacity is also required in the process model of the second (Unscented) Kalman filter. It is possible to take the nominal capacity or any other recent measurement result. In this study, the actual relative cell capacity $C_{\mathrm{rel},k} = C_{\mathrm{cell},k}/C_{\mathrm{BOT}}$ is estimated by ε-SVR, where C_{BOT} is the begin-of-test (BOT) capacity, and serves as an input value for the model parameter in the second Kalman filter. The data for the SVR was obtained from the long-term cell ageing tests (i).

The composition of the input vector can be seen in Table 4 with an additional scaling to [−1,1] for temperatures and [0,1] for the other features [15].

Multiple data vectors were created for every check-up of every cell, such that every time interval between a check-up and all previous check-ups including the BOT measurement is accounted.

Table 3
Equations for filter 2 (UKF).

$$\boldsymbol{x}_k = \begin{pmatrix} \mathrm{SOC}_k \\ R_{1,k} \\ R_{2,k} \end{pmatrix}$$

$$u_k = I_k$$

$$\boldsymbol{z}_k = \begin{pmatrix} U_{\mathrm{cell},k} - U_{1,k} - U_{2,k} - U_{\mathrm{ohm},k} \\ U_{1,k} \\ U_{2,k} \end{pmatrix}$$

$$\boldsymbol{x}_{k+1} = \boldsymbol{x}_k + \begin{pmatrix} \frac{\Delta t_{k+1}}{C_{\mathrm{cell}}} \\ 0 \\ 0 \end{pmatrix} \cdot u_k$$

$$\boldsymbol{z}_k = \begin{pmatrix} U_{\mathrm{OCV}}(x_{1,k}) \\ U_{1,k-1} \cdot e^{-\frac{\Delta t_k}{\tau_1}} + x_{2,k} \cdot \left(1 - e^{-\frac{\Delta t_k}{\tau_1}}\right) \cdot I_{k-1} \\ U_{2,k-1} \cdot e^{-\frac{\Delta t_k}{\tau_2}} + x_{3,k} \cdot \left(1 - e^{-\frac{\Delta t_k}{\tau_2}}\right) \cdot I_{k-1} \end{pmatrix}$$

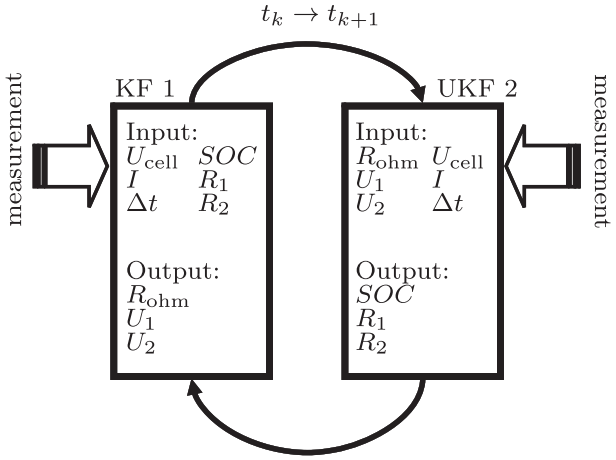

Fig. 4. Design of the dual Kalman filter with estimated states, required inputs and interactions of the filters.

In this way a number of 1899 training vectors and 566 testing vectors was obtained.

The choice of the required ε-SVR parameters can be seen in Table 4, where the value of ε was chosen because of the expected measurement error and cell spread. The kernel function parameter $\tilde{\sigma} = 1/2\sigma^2$ and the regularization constant C were obtained by grid search and 5-fold cross validation [15] based on the training data.

The SVR part is used offline and the ideas are that new training data can be fed into the model e.g. regularly when a full charge is performed or at regular services.

In addition, the SVR could also be used to obtain initial values for the resistances estimated in the DKF or to deliver estimates of the state of health on its own.

A very interesting further application of the SVR would be to determine the parameters of an equation describing the ageing or the lifetime instead of predicting the capacity directly. A possible equation would be e.g:

$$C_{\mathrm{actual}} = C_{\mathrm{BOL}} \cdot \left(100 - \alpha \cdot t^{\beta} - \eta \cdot Ah_{\mathrm{throughput}}\right) \tag{16}$$

Table 4
Data structure and set parameters of the support vector regression.

Variable	Description
(a) Composition of the data vectors	
Input vector	
$C_{\mathrm{rel},t1}$	Relative cell capacity at time t_1
T_{min}	Minimal temperature
T_{max}	Maximal temperature
$d = t_2 - t_1$	Time span
I_{mean}	Mean current rate
q	Amount of charge and discharge
$\mathrm{SOC}_{\mathrm{max}}$	Maximal SOC
Δ_{SOC}	SOC lift
Target value	
C_{rel,t_2}	Relative cell capacity at time t_2
SVR parameter	Value
(b) Initialised parameters	
Kernel function $k(x,y)$	$\exp\left(-\frac{\|x-y\|^2}{2\sigma^2}\right)$ where $1/2\sigma^2 = 2.9$
ε	0.005
C	60

to describe the capacity fade over calendar and cycle life. The dependency of the parameters on the operation conditions could now be obtained by the SVR. This approach was tested and showed also very satisfying results for the training as well as the validation with unknown ageing conditions. Two main advantages can be found for this indirect approach. First, measurements inaccuracies are compensated and the estimation is more robust against measurement errors or noise. Second, by obtaining these parameters an additional prognosis is possible. Especially, if a large number of ageing test is available, the parameters are well suited for a lifetime prediction.

In this study, the SOH is not predicted directly, but can be calculated from the estimated actual cell capacity and the ohmic resistance defining specific end-of-life criteria. Here, the SOH will be defined the following way:

$$\mathrm{SOH} := \begin{cases} 100\% & \mathrm{begin-of-life(BOL)} \\ 0\% & \mathrm{end-of-life(EOL)} \\ \mathrm{linear\ interpolated\ in\ between} \end{cases}$$

with the following typical automotive EOL criteria:

$$R_{\mathrm{EOL}} = 2 \cdot R_{\mathrm{BOL}}$$
$$C_{\mathrm{EOL}} = 0.8 \cdot C_{\mathrm{BOL}}$$

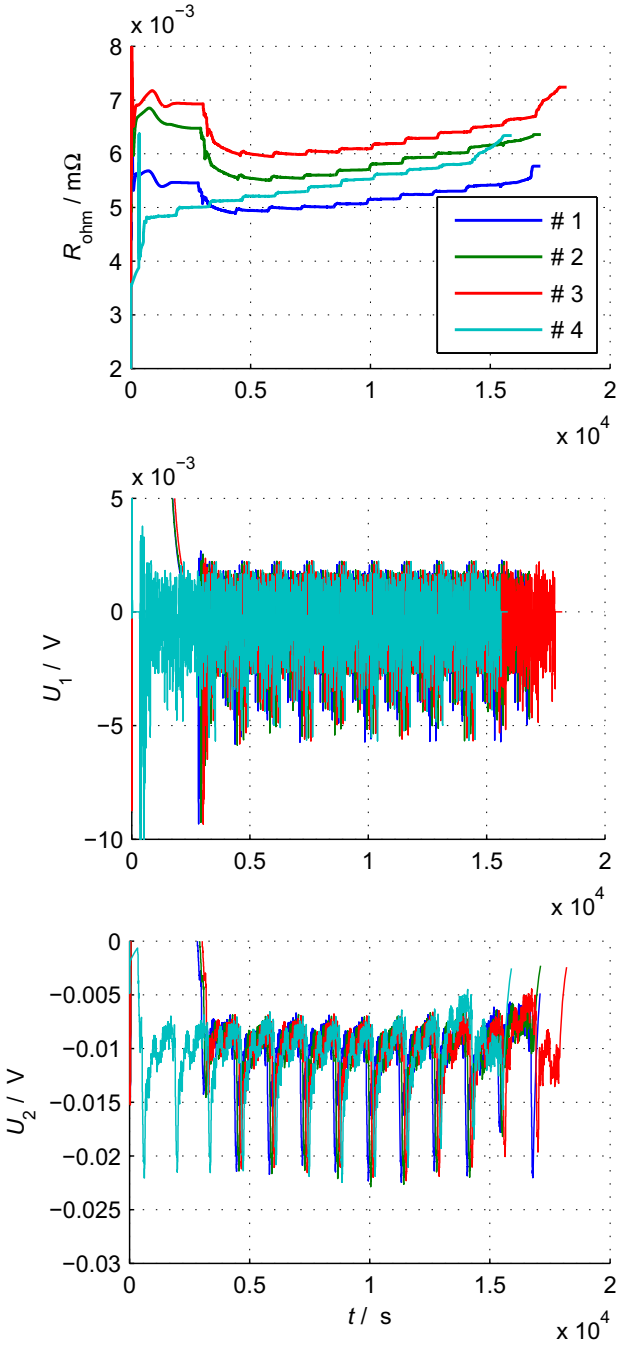

Fig. 5. During a drive cycle estimated ohmic resistance and over voltages of four cells with different capacity SOH (blue line 94.5%, green line 90.0%, red line 95.2%, light blue line 98.0%) by the first Kalman filter. (For interpretation of the references to colour in this figure legend, the reader is referred to the web version of this article.)

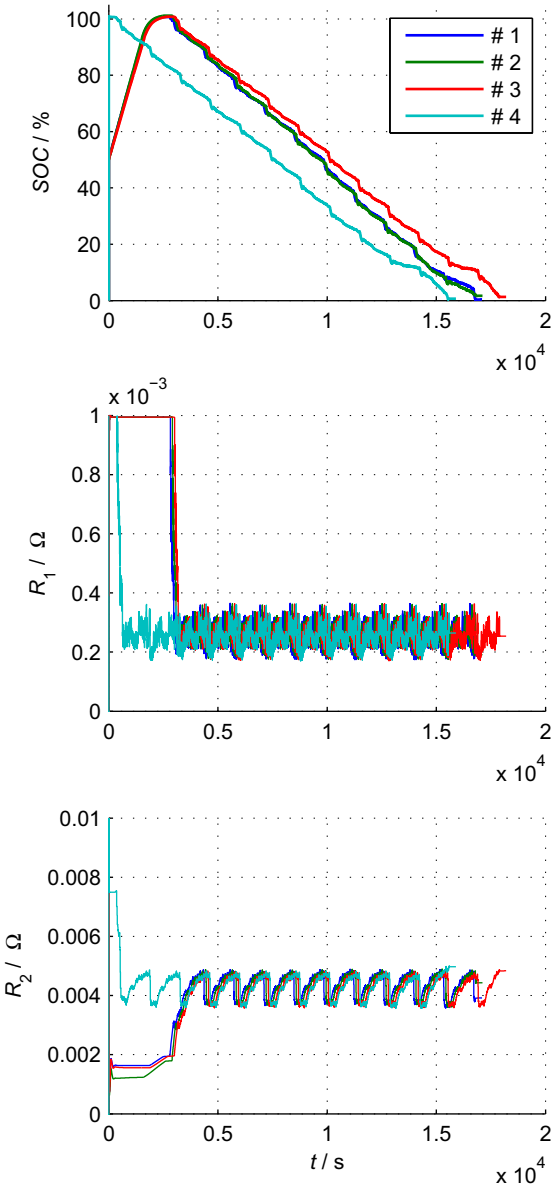

Fig. 6. During a drive cycle estimated SOC, polarization resistance and diffusion resistance of four cells with different capacity SOH by the second Kalman filter.

Both, the Dual Filter and the support vector regression have been implemented in MATLAB code, where a common SVM toolbox, LIBSVM [16], is used for the SVR part.

5. Results and discussion

The driving cycle measurement data (ii.a) is first applied to the dual filter algorithm. The estimated states over time for four different cells are plotted in Figs. 5 and 6 for filter 1 (KF) and filter 2 (UKF), respectively. It can be seen, that the ohmic resistance estimate R_{ohm} varies clearly between the differently aged cells and it increases as expected with decreasing state-of-charge.

The SOC estimate shows very uniform characteristics starting with a value 100%SOC and ending with almost 0%SOC. Especially, comparing the curve of cell two and three, a different cell capacity can be guessed.

Also, the evolution of the over-voltages U_1 and U_2 over time seem feasible, but cannot be validated directly. However, two interesting points are obviously. First, the same trends of the over-voltages is found for all four cells and second, the over-voltage due to diffusion is four times higher than due the polarization effect. For the resistances R_1 and R_2 a little noisy behaviour in a fixed constant range of 0.2–0.3 mΩ and 4–5 mΩ, respectively, independently of initial values or the type of driving cycle measurement is found. In contrast to R_{ohm}, no significant influence of the SOH is visible.

Since the concrete values of the over-voltages U_1 and U_2 and the corresponding resistances R_1 and R_2 are not essential, only the SOC and R_{ohm} estimates for the second driving cycle measurement (ii.b) are shown. The evolution over time for those two states is given by Fig. 7a and b, respectively.

Again, the ohmic resistance of the investigated cells shows similar but shifted curves. Also the SOC of the four cells over the drive cycle, starting at different times due to visibility, show almost identical trends. However, a deeper look at the reached SOC level during both pauses shows slightly different values. This is caused by the different capacity SOH of the cells and can be evaluated. To

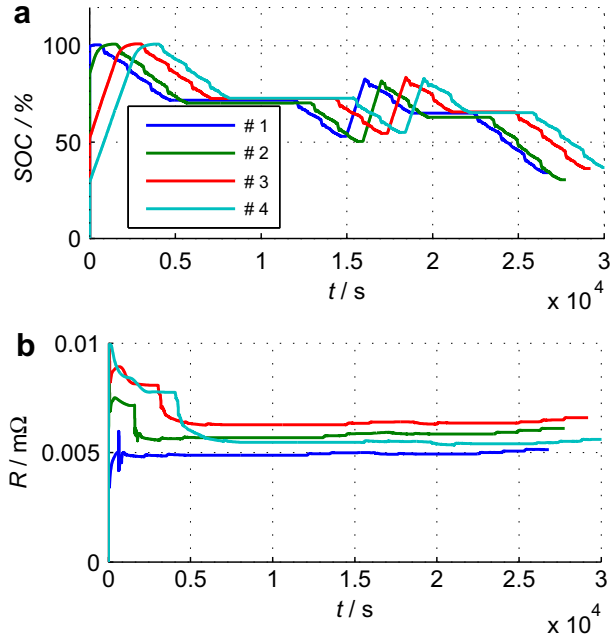

Fig. 7. Estimation of SOC and R_{ohm} during cycling (type ii.b) for four cells with different capacity SOH with an initial value of $C_{cell} = C_{cell,\ actual}$. (a) Estimated SOC. (b) Estimated R_{ohm}.

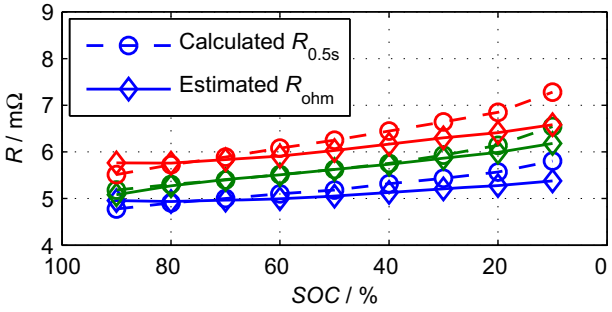

Fig. 8. Comparison of calculated (dashed line with circles) and estimated (solid lines with triangles) ohmic resistance of three cells with different resistance SOH (red line 127%, green line 108%, blue line 101%). (For interpretation of the references to colour in this figure legend, the reader is referred to the web version of this article.)

validate the results of applied dual filter, the PPCP test of Section 3 is used including the SOC–OCV curves as well as the time dependent resistance of Eq. (12) of each cell. Since the voltage drop caused by the ohmic resistance happens instantaneously, one tries to account the voltage difference of the smallest analysable time difference. In this case, the smallest time residual for the measurement was 0.5 s and will contain also polarization effects. Nevertheless, this resistance is in a small range as demonstrated in Fig. 6 and consequently $R_{0.5\ s}$ provides a good approximation for the ohmic resistance.

It is therefore possible to validate the state estimates SOC and R_{ohm} with the measured open-current voltages after relaxation and the calculated $R_{0.5\ s}$ resistances, respectively. Obviously, only the SOC estimates at the rest periods of the second drive cycle measurement (ii.b) can be validated. The ohmic resistance estimate R_{ohm} will be validated comparing the results of the first driving cycle measurement (ii.a), because it covers the whole SOC range from 100%SOC to almost 0%SOC with the calculated $R_{0.5\ s}$ resistance based on the PPCP measurements.

A comparison of the calculated and the estimated resistance values over state of charge for three selected cells is given by Fig. 8. Both resistances show similar characteristics with a slightly different gradient. The calculated resistances show a higher increase with decreasing SOC compared to the estimates. This is explainable with the voltage drop caused by the OCV decrease when discharging the cell, which is accounted in the dual filter model but not in the calculation. The lower the SOC, the higher the OCV decrease and therefore the difference in the resistances.

Table 5
Estimates SOC_{est} and deviation ΔSOC from the measurement value SOC_{actual} for different start values of C_{cell}.

	Cell 1	Cell 2	Cell 3	Cell 4
(a) Estimated SOC and deviation ΔSOC from the measured value at the end of the first rest period				
SOC_{act}	72.35	70.85	72.96	73.55
$SOC_{est}(C_{cell,a})$	71.79	70.33	72.66	72.86
ΔSOC	0.56	0.52	0.30	0.69
$SOC_{est}(C_{cell,1} = 8\ Ah)$	71.64	70.20	72.47	72.60
ΔSOC	0.71	0.65	0.49	0.95
$SOC_{est}(C_{cell,2} = 12\ Ah)$	71.91	70.49	72.78	72.97
ΔSOC	0.44	0.36	0.18	0.58
(b) Estimated SOC and deviation ΔSOC from the measured value at the end of the second rest period				
SOC_{act}	65.06	63.06	65.80	65.40
$SOC_{est}(C_{cell,a})$	65.04	62.88	65.70	65.35
ΔSOC	0.02	0.18	0.10	0.05
$SOC_{est}(C_{cell,1} = 8\ Ah)$	64.84	62.70	65.49	65.13
ΔSOC	0.22	0.36	0.31	0.27
$SOC_{est}(C_{cell,2} = 12\ Ah)$	65.19	63.10	65.84	65.45
ΔSOC	0.13	0.04	0.04	0.05

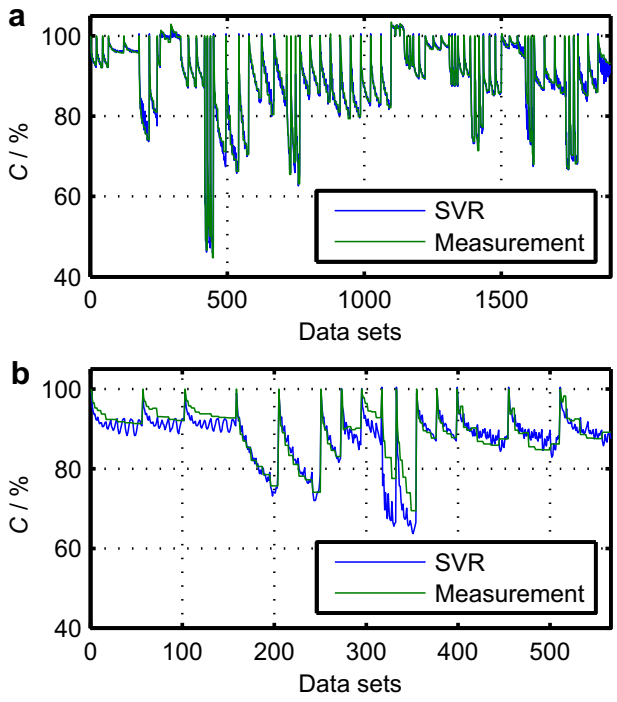

Fig. 9. Validation of the SVR training (a) and capacity prediction (b) by comparison of SVR (blue line) to calendar and cycling ageing measurements (green line). (a) Training of the SVR. (b) Prediction by SVR. (For interpretation of the references to colour in this figure legend, the reader is referred to the web version of this article.)

Subsequently, a very good quality of the resistance estimate can be followed too.

Table 5 shows the SOC estimates for three different values for the cell capacity model parameter C_{cell}, where $C_{cell,a}$ is the actual "true" cell capacity obtained from capacity tests and $C_{cell,1}$ and $C_{cell,2}$ are fixed values, which are up to 20% lower and higher, respectively.

It can be seen, that the maximal deviation of the SOC estimate from the true value is under 1%, even if the model parameter cell capacity C_{cell} has 20% deviation from the true value. By assuming again a consistent form of the OCV-curve over lifetime, the actual cell capacity can now be calculated easily by using the OCV/SOC relation and the discharged Ah-amount.

Now, the possibility to obtain an initial C_{cell} for the DKF by the use of SVR, is tested and validated with regard of a maximum error limit of 20% for an unknown cell history. As mentioned before, a total of almost two thousand data vectors from ageing tests (i) was applied in order to train the SVR. A very successful training is achieved as evidenced by Fig. 9a. The curve of all storage and cycling ageing tests is reproduced by the SVR throughout with a high accuracy. Afterwards, the SVR model is used to predict six ageing scenarios which were not part of the training. Also this validation shows a high accuracy as illustrated in Fig. 9b. The overall trend of all cells is reproduced correctly and just small deviations, with an average error in the range of the cell spread between the three tested cells, can be found. Looking at the maximum error, even for the strongest degradation a value below 20% is reached. Thus, the predicted capacity is outstandingly suitable to be used as an input value for the dual Kalman Filter.

6. Conclusions

In this study a robust and powerful real-time SOC and SOH estimation for lithium-ion batteries has been developed. It was shown, how the mathematical methods, namely minimum variance estimation and machine learning, can be combined for this purpose. The performance of the resistance and SOC estimation have been validated using results of pulse power characterization tests and the open-current voltage curves, respectively.

The accuracy of the SOC and resistance estimation can be regarded superior to existing publications. Even with a capacity error of 20%, the DKF showed excellent results with an SOC estimation error below 1% as well as comprehensible values for all resistances in case of realistic drive cycles. Moreover, it was showed that the SVR can be used offline to gain a convenient initial capacity for the DKF or even for lifetime prediction.

In a next step, the realization of the algorithms on a BMS should be evaluated in terms of computation and accuracy for vehicle data instead of laboratory data.

References

[1] J. Vetter, P. Novák, M. Wagner, C. Veit, K.-C. Möller, et al., Journal of Power Sources 147 (1–2) (2005) 269–281.
[2] G. Plett, Journal of Power Sources 134 (2004) 252–292.
[3] G. Plett, Journal of Power Sources 161 (2006) 1356–1384.
[4] T. Hansen, C.-J. Wang, Journal of Power Sources 141 (2005) 351–358.
[5] A. Widodo, M.-C. Shim, W. Caesarendra, B.-S. Yang, Expert Systems with Applications 38 (2011) 11763–11769.
[6] B. Saha, K. Goebel, S. Poll, J. Christophersen, IEEE Transactions on Instrumentation and Measurement 58 (2009) 291–296.
[7] J. Zhang, J. Lee, Journal of Power Sources 196 (2011) 6007–6014.
[8] R.E. Kalman, Transactions of the ASME – Journal of Basic Engineering 82 (Series D) (1960) 35–45.
[9] G. Welch, G. Bishop, An Introduction to the Kalman Filter, Tech. Rep., Chapel Hill, NC, USA, 1995.
[10] S. Julier, J. Uhlmann, A new extension of the Kalman filter to nonlinear systems, in: Int. Symp. Aerospace/Defense Sensing, Simul. and Controls, Orlando, FL, 1997.
[11] A.J. Smola, B. Schölkopf, Statistics and Computing 14 (3) (2004) 199–222.
[12] Idaho National Engineering and Environmental Laboratory, FreedomCAR Battery Test Manual For Power-assist Hybrid Electric Vehicles, DOE/ID-11069.
[13] D. Andre, M. Meiler, K. Steiner, C. Wimmer, T. Soczka-Guth, D. Sauer, Journal of Power Sources 196 (12) (2011) 5334–5341.
[14] H. Dai, X. Wei, Z. Sun, J. Wang, W. Gu, Applied Energy 95 (0) (2012) 227–237.
[15] C.-W. Hsu, C.-C. Chang, C.-J. Lin, A Practical Guide to Support Vector Classification, National Taiwan University, 2010.
[16] C.-C. Chang, C.-J. Lin, Libsvm: A Library for Support Vector Machines (2001).